

Yoshinobu Tsujimoto
Professor.

Yoshiki Yoshida
Assistant Professor.

Osaka University, Engineering Science,
1-3 Machikaneyama, Toyonaka, 560,
Japan

Hideo Ohashi
President,
Kogakuin University, Mechanical
Engineering, Nishishinjuku 1-24-2,
Shinjuku, Tokyo, 163-91, Japan

Norihiro Teramoto
Engineer, Kubota Corporation

Shin Ishizaki
Engineer, Ishikawajima Harima Heavy
Industries, Inc.

Fluid Force Moment on a Centrifugal Impeller Shroud in Precessing Motion

Experimental results of fluid moment on a centrifugal impeller shroud in precessing motion are discussed based on the bulk flow model to elucidate the fundamental flow mechanism. It is shown that the backshroud/casing clearance flow and the destabilizing fluid force moment can be simulated by the bulk flow model fairly well if the measured behavior of the resistance is correctly incorporated in the model. From the calculations with and without steady and unsteady wall shear stresses, the unsteady component of the clearance flow is shown to be basically a two-dimensional inviscid flow induced by the change in the flow thickness. The effects of the leakage flow rate and the resistance at the leakage flow entry are discussed, paying attention to the steady tangential velocity of the leakage flow.

Introduction

For rotordynamic problems, forces on seals and bearings play important roles. For these problems, see Childs' textbook (1993). For turbomachinery operating at supercritical shaft speed it is also important to understand the characters of unsteady fluid forces on the impeller which occur in response to shaft vibration. They are called "rotordynamic forces (Brennen, 1994)" and considerable knowledge has been obtained for whirling closed type centrifugal impellers. Although the impeller whirling forces are basically stabilizing the rotor vibration (Ohashi and Shoji 1987, Shoji and Ohashi 1987), they become destabilizing under the following conditions: (i) at reduced flow rate (Ohashi and Shoji, 1987, Tsujimoto and Acosta, 1987), (ii) when there is interaction with volute or vaned diffuser (Jery et al., 1985; Adkins and Brennen, 1988; Tsujimoto et al., 1988A, 1988B) or (iii) when the clearance between front shroud and casing of 3-D impeller is small (Jery, 1986; Ohashi et al., 1988; Bolleter et al., 1987; Guinzburg et al., 1994; Childs, 1989). The importance of the shroud/casing clearance flow was shown recently by Smith et al. (1996) from their field experiences.

For precessing motion, Ohashi et al. (1991) have shown that, from direct force measurements, the fluid force moment may become destabilizing for the precessing velocity ratio $0 \leq \Omega/\omega \leq 0.5$. This destabilizing velocity ratio range is quite similar that of whirling cases mentioned in the last paragraph. The present paper focuses on the backshroud/casing clearance flow and attempts have been made to explain the flow mechanism based on the bulk flow model, originally applied by Childs (1989) to estimate the whirling shroud forces. In the present study, the precessing shroud force moments are evaluated from unsteady pressure measurements, which includes the effects of the leakage flow rate and the flow resistance at the entrance of the leakage flow path. In addition, unsteady pressure and velocity field measurements are conducted and the results are com-

pared with those of the bulk flow model. The experimental results are partly reported elsewhere (Yoshida et al., 1996) but the discussions on the flow mechanisms are made in the present paper based on the bulk flow model.

Outline of Experiments

Figure 1(a) shows the experimental apparatus. The impeller is a model of a boiler feed pump with outer radius $R_i = 165$ mm, width $b_2 = 28$ mm, and vane angle from tangent = 24.5 deg and design flow coefficient $\phi_d = 0.106$. Details of the apparatus have been reported by Ohashi et al. (1991). The center of the precessing motion is set at O, the intersection of the centerline of the untilted impeller with the central plane of the impeller discharge. The axis of the impeller executes a precessing motion with a constant precessing angular frequency Ω keeping the apex angle to be $\alpha = 0.9$ deg. The rotational speed of the main shaft is kept to be 677 rpm ($=60\omega/2\pi$) and the precessing velocity ratio Ω/ω is changed between -1.4 and 1.4. Air is used as the working fluid. The flow from the impeller is discharged to a vaneless diffuser of radius ratio 1.45 and then to a circular collector, as shown in Fig. 1(b).

Although the leakage in the backshroud clearance in boiler feed pump is radially outward, inward leakage flow is assumed in this study since it is more common in other types of the pumps. The unsteady pressure is measured using the pressure taps C-F. The unsteady velocity measurements are made at the same radial locations as the pressure taps, by using a hot wire anemometer. The clearance S at the leakage flow entrance is changed to be $S = 1, 2$ and 5 mm. The backshroud/casing clearance at normal position is set to be $H_0 = 7.5$ mm. The circumferential Reynolds number at the leakage flow entry (at impeller outer radius R_i) based on the clearance H_0 was $R_i\omega H_0/\nu = 5850$, and the radial Reynolds number range $U_r H_0/\nu = 0 \sim 193$, where U_r is mean radial velocity at the leakage flow entrance due to leakage flow. The leakage flow exit G is connected to a blower to produce the leakage flow through a flow meter and a flow control valve.

Figure 2 shows the coordinate system. The r -axis is set in the direction of maximum clearance and the t -axis perpendicular

Contributed by the Fluids Engineering Division for publication in the JOURNAL OF FLUIDS ENGINEERING. Manuscript received by the Fluids Engineering Division April 26, 1996; revised manuscript received January 7, 1997. Associate Technical Editor: B. Schiavello.

to it, proceeding by 90 degs from r -axis in the direction of impeller rotation. The precessing angular velocity Ω is positive when it is in the same direction as the impeller rotation ω . The fluid moment M is represented with its radial (M_r) and tangential (M_t) components. For the cases when M_r has the same sign as Ω/ω , it has the effects to promote the precessing motion in the direction of Ω , (with the opposite sign, to damp). On the other hand, $M_t > 0$ shows the moment which has the same effect as the increase of shaft stiffness for bending, for overhung rotor. The moments M_r and M_t are normalized with $M_0 = I\alpha\omega^2$, where $I = \rho\pi R_i^2 b_2^2 i^2$ with $i = \sqrt{R_i^2/4 + b_2^2/12}$ is the moment of inertia of hypothetical fluid disk of thickness b_2 and radius R_i , around the diameter.

Bulk Flow Model

The bulk flow model was first applied by Childs (1989) to estimate the forces on the front shroud of a whirling centrifugal impeller and later by Guinzburg (1994) on a model rotor. The details are not reproduced here. This model assumes a two-dimensional inviscid flow with variable flow thickness H , in which the (empirical) wall shear stress is taken into account as an external body force. The momentum and continuity equations are linearized assuming that the unsteady components of flow thickness, pressure and velocity are sufficiently small. In the present study, the fundamental equations are integrated numerically so as to satisfy the following boundary conditions.

At the leakage flow inlet ($R = R_i = 165$ mm, see Figs. 1 and 5)

(For steady component, represented with suffix 0)

- (a) Radial velocity U_{R0} is given from assumed leakage flow rate
- (b) Tangential velocity $U_{\theta 0} = 0.5 R_i \omega$, caused by equal steady wall friction on both sides of the inlet clearance.
- (c) Pressure P_0 can be given arbitrarily as a reference pressure.

(For unsteady component, represented with suffix 1)

- (d) Unsteady tangential velocity $U_{\theta 1} = 0$, resulting from uniform circumferential distribution of wall friction at the inlet.
- (e) Resistance at the inlet is represented by $P_1/\rho = F(U_{R1})$, the functional form of F is discussed later.

At the leakage flow outlet ($R = R_o = 32.5$ mm, see Fig. 1)

(For unsteady component)

- (f) Constant pressure $P_1 = 0$ is assumed since the leakage flow exits to a relatively large space without flow restriction.

The shear stress representation as proposed by Hirs (1973) is used with Yamada's empirical factors (1962) in the following calculations.

Results and Discussions

The results are shown only for design pump flow coefficient $\phi_d = 0.106$, since it was found that the effects of pump flow rate was quite small. This suggests the validity of the boundary condition (b).

Velocity Distribution Across the Clearance. Figure 3 shows the mean velocity distribution and the amplitude of velocity fluctuation caused by the precessing motion with $\Omega/\omega = 0.2$ and 1, with the leakage flow coefficient $\phi_l = 0$ and the clearance $S = 2$ mm. The measurements are made at location E ($R = 100$ mm, $R/R_i = 0.606$) in Fig. 1. The range of backshroud movement is shown in the figure. The average of the mean tangential velocity is $U_{\theta}/R\omega \approx 0.5$. Small inward velocity (i.e., $U_r < 0$) due to secondary flow is observed near the casing wall but $U_r/R\omega \approx 0$ at the center of the clearance. The amplitude of the velocity fluctuation is relatively uniform over the clearance and it was confirmed that the phase was nearly constant. From this measurement it is expected that the bulk flow model is a good approximation of the clearance flow.

Effects of Loss at the Inlet of Leakage Flow Path. It is generally assumed that the pressure loss ΔP at the inlet is proportional to U_R^2 :

$$\Delta P/\rho = (1 + \xi)(-U_R)^2 \quad (1)$$

The perturbation of this relation gives

$$P_1/\rho = F(U_{R1}) = -(1 + \xi)U_{R0}U_{R1} \quad (2)$$

which gives zero pressure fluctuation ($P_1 = 0$) for the case without leakage ($\phi_l = 0$, $U_{R0} = 0$) irrespective of the value of loss coefficient ξ . Figure 4 shows the comparison of the results of experiment and calculations with the assumption of Eq. (1). The calculation underpredicts the moments significantly.

Under this situation the loss is experimentally examined. Figure 5 shows the dependence of loss on the leakage flow coefficient ϕ_l . (The circumferential Reynolds number $R_i\omega S/\nu$ ($S = 2$ mm) is 1560 and the Reynolds number in the flow direction $V_m S/\nu$ is from 0 to 193 in the experiment.) The pressure loss is estimated from the pressure measurements at pressure taps

Nomenclature

b_2 = impeller outlet width (see Fig. 5)
 H = flow thickness
 H_0 = casing/backshroud clearance
 j = imaginary unit
 K = proportionality constant, Eq. (3)
 M_r = radial component of fluid force moment
 M_t = tangential component of fluid force moment
 P = pressure
 ΔP = pressure loss at the leakage flow entry
 R = radial coordinate
 S = clearance at the leakage flow entry

t = time
 U_R, U_{θ} = radial (positive outward) and circumferential (positive in the direction of impeller rotation) velocity
 V_m = mean velocity at the inlet clearance
 α = apex angle of precessing motion
 ξ = loss coefficient
 θ = circumferential coordinate
 μ = viscosity
 ν = kinematic viscosity
 ρ = density
 ϕ = pump flow coefficient, = pump flow rate/ $(2\pi R_i^2 b_2 \omega)$

ϕ_l = leakage flow coefficient, = leakage flow rate/ $(2\pi R_i^2 b_2 \omega)$
 ω = angular velocity of impeller rotation
 Ω = angular velocity of precessing motion

Suffix

0 = steady component
 1 = unsteady component
 i = inlet to the leakage flow path, at the outer radius of the impeller (see Fig. 1)
 o = exit from the leakage flow path, at the inner radius of the impeller (see Fig. 1)
 r = radial component (see Fig. 2)
 t = tangential component (see Fig. 2)

S=1, 2, 5(mm)

A-F: pressure and velocity measurement locations

G: leakage flow exit

O: center of precession

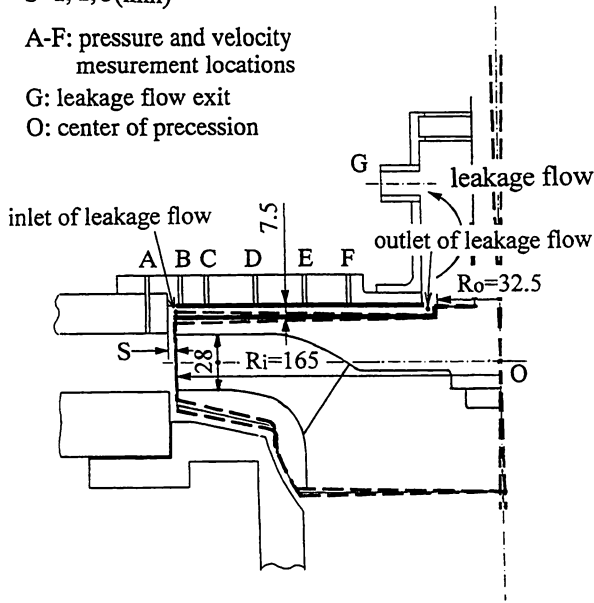


Fig. 1(a) Details around the impeller

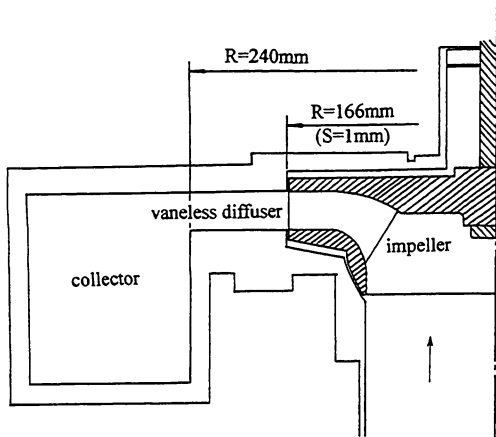


Fig. 1(b) Cross section of the pump (impeller, vaneless diffuser, and collector)

Fig. 1 Experimental apparatus

A ($R/R_i = 1.09$) and B ($R/R_i = 0.989$), taking into account the effect of centrifugal force due to swirl. The loss is rather linear with ϕ_i than parabolic as expected from Eq. (1). For the case with $S = 1$ mm, the loss can be estimated as the sum of pressure loss of Poiseuille flow and the dynamic pressure of the mean leakage flow. However, this gives smaller loss for larger clearance. Even at $\phi_i = 0$, the linear curves have finite slope and thus the inlet pressure P_1 has nonzero value unlike the relation of Eq. (2).

Based on this result the relation

$$P_1/\rho = F(U_{R1}) = KU_{R1} \quad (3)$$

has been used for the boundary condition (e) with K estimated from the slope of the $\Delta P - \phi_i$ curve. The full line in Fig. 6 shows the result under this boundary condition. We observe reasonable agreement. We should note that the destabilizing moment $M_r > 0$ in $0 < \Omega/\omega < 0.5$ is nicely simulated.

The velocity and pressure fluctuation fields as viewed from casing are shown in Fig. 7. The velocity fluctuation is measured at 3 mm from casing in the 7.5 mm casing/backshroud clearance. The direction r is defined as the direction with maximum clearance. These patterns rotate with the angular velocity Ω of

the precessing motion. The pressure distribution on the backshroud was integrated to estimate the fluid force moments M_r and M_t . The experiment and the calculation agree fairly well including their phase relationships.

The above discussions show that the bulk flow model can estimate both the flow field and the resulting force moment once the correct behavior of the inlet loss is used, for the cases with the size of the clearance of the present study.

Effects of Wall Shear Stress. In the perturbation analysis using the bulk flow model, the wall shear stress can be separated into steady (time mean) and unsteady (perturbation) components. Figure 6 compares the results of calculations under the following three conditions, without leakage flow: (1) with steady and unsteady shear stress, (2) with steady but without unsteady stress, and (3) without steady and unsteady shear stress. The steady shear stress controls the steady tangential velocity distribution. Without leakage flow, the tangential velocity becomes $U_{\theta 0} = 0.5 R\omega$ so long as the shear stresses on the casing wall and the backshroud have the same value, irrespective of their magnitude. This tangential velocity distribution is used for the cases of (1) and (2). Without steady shear stress and leakage, $U_{\theta 0}$ can be assumed arbitrarily. However, if we consider an infinitesimal leakage, the steady velocity is deter-

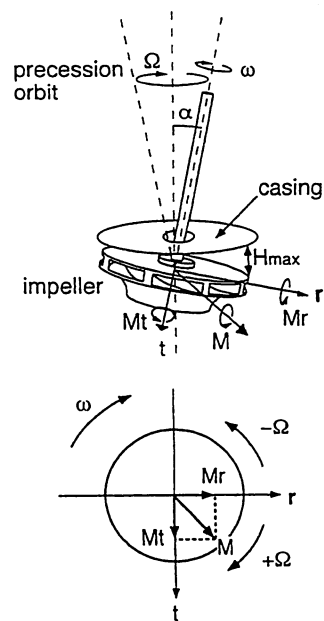


Fig. 2 Coordinate system

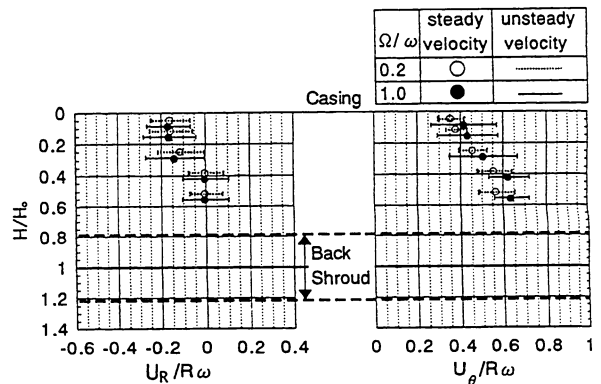


Fig. 3 Velocity distribution over the clearance (normalized by local circumferential velocity $R\omega$ at location E, $R/R_i = 0.606$, $\phi_i = 0$, $S = 2$ mm, uncertainty in velocity measurement is $U_R, U_\theta/R\omega = \pm 0.01$)

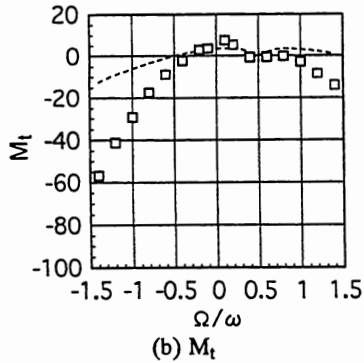
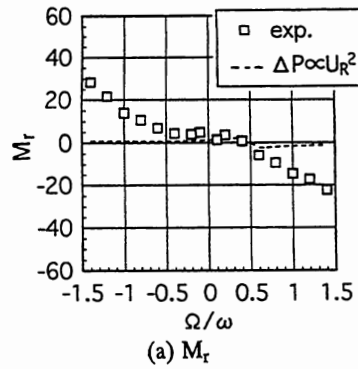


Fig. 4 Normalized moment components (with $\Delta P \propto U_R^2$, $\phi_i = 0$, $S = 2$ mm, uncertainty in M_r , $M_t = \pm 2$ and in $\Omega/\omega = \pm 0.002$)

mined from the conservation of angular momentum and can be written as $U_{\theta 0} = 0.5(R_i^2/R)\omega$ if we assume that $U_{\theta 0} = 0.5 R_i \omega$ at the inlet. This distribution has been used for the calculation of the case (3).

The comparison of the cases (1) and (2) shows that the unsteady shear stress has little effect on the moment components. However, the result of (3) shows that the steady shear stress, i.e., the steady tangential velocity distribution has a large

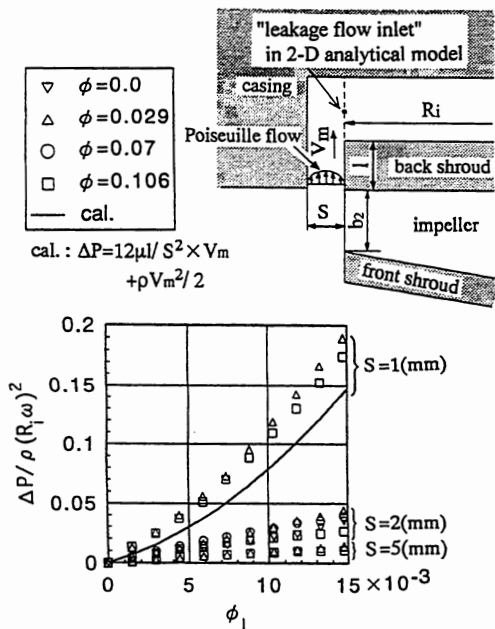


Fig. 5 Pressure loss at the leakage flow inlet (uncertainty in $\Delta P / \rho(R_i \omega)^2 = \pm 0.005$, in $\phi_i = \pm 0.5 \times 10^{-3}$)

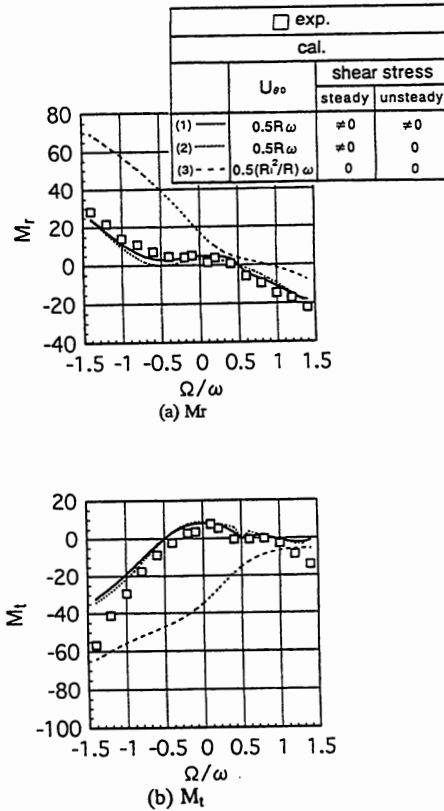


Fig. 6 Normalized moment components (effects of wall shear stress, with $\phi_i = 0$, $S = 2$ mm, uncertainty in M_r , $M_t = \pm 2$ and in $\Omega/\omega = \pm 0.002$)

effect on the moment. These results suggest that the unsteady component is basically a two-dimensional inviscid flow affected by fluid viscosity through the steady tangential velocity distribution and through the pressure loss at the leakage flow entry. The viscosity of the fluid affects the fluid moment through the steady tangential velocity distribution as shown here and through the pressure loss at the leakage flow.

Under the simplifying assumptions of: (a) unsteady wall shear stress can be neglected, (b) flat clearance flow surface with constant flow thickness, (c) no leakage flow—forced vor-

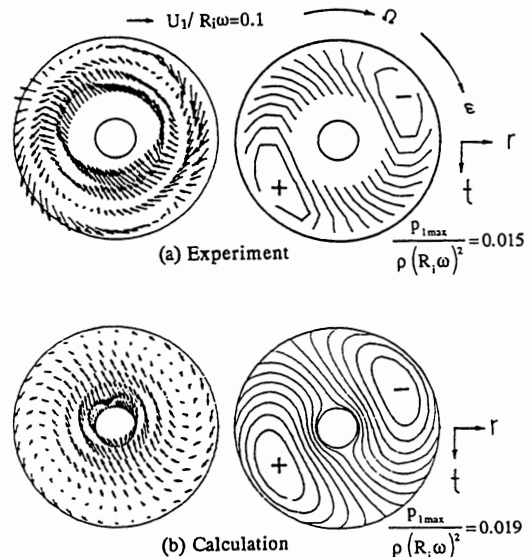


Fig. 7 Velocity and pressure fluctuation fields ($\phi_i = 0$, $S = 2$ mm, $\Omega/\omega = 0.2$, uncertainty in $U_i / (R_i \omega) = \pm 0.01$, in $P_i / \rho(R_i \omega)^2 = \pm 0.001$)

text distribution of steady tangential velocity $U_{\theta 0} = R\omega^*$. (The number of ω^* would depend on the shear stresses on the shroud and casing. For the case with equal stresses $\omega^* = 0.5\omega$.) The following semi-analytical representation of the flow disturbance can be obtained for the precessing motion with $H = R\alpha e^{j(\Omega t - \theta)}$:

$$U_{R1} = [C_1 R^2 + C_2 R^{-2} + C_3] e^{j(\Omega t - \theta)} \quad (4)$$

$$U_{\theta 1} = (\Omega - \omega^*)(R^2 \alpha / H_0) e^{j(\Omega t - \theta)} - j(R \frac{\partial U_{R1}}{\partial R} + U_{R1}) \quad (5)$$

$$P_1 = -\rho j \{ j(\Omega - \omega^*) U_{\theta 1} + 2\omega^* U_{R1} \} R \quad (6)$$

where

$$C_1 = -j(3\Omega - 5\omega^*)(\alpha / H_0) / 8$$

and C_2 and C_3 are determined from the boundary conditions ($P_1 / \rho = K_i U_{R1}$ at $R = R_i$ and $P_1 / \rho = K_o U_{R1}$ at $R = R_o$) which can be rewritten as

$$\begin{bmatrix} -j(-\Omega + 3\omega^*)R_o^{-1} - K_o R_o^{-2} - j(\Omega + \omega^*)R_o - K_o \\ -j(-\Omega + 3\omega^*)R_i^{-1} - K_i R_i^{-2} - j(\Omega + \omega^*)R_i - K_i \end{bmatrix} \begin{pmatrix} C_2 \\ C_3 \end{pmatrix} = \begin{bmatrix} j \{ j(\Omega - \omega^*)^2 R_o^2 (\alpha / H_0) + (3\Omega - \omega^*) C_1 R_o^2 \} + K_o C_1 R_o^2 \\ j \{ j(\Omega - \omega^*)^2 R_i^2 (\alpha / H_0) + (3\Omega - \omega^*) C_1 R_i^2 \} + K_i C_1 R_i^2 \end{bmatrix} \quad (7)$$

The fluid force moment can be given by (in dimensional form)

$$\begin{aligned} -M_r + jM_t &= -\rho \pi j \{ j(\Omega + \omega^*)(3\omega^* - \Omega) \\ &\times (R_i^6 - R_o^6) / (4H_0) + C_3(\Omega + \omega^*)(R_i^4 - R_o^4) / 4 \\ &+ C_2(3\omega^* - \Omega)(R_i^2 - R_o^2) / 2 \} \quad (8) \end{aligned}$$

We should note that the amplitudes of unsteady flow components and the fluid force moment are inversely proportional to the steady clearance H_0 . With $\omega^* = 0.5\omega$, the above results agree with the case (2) in Fig. 6.

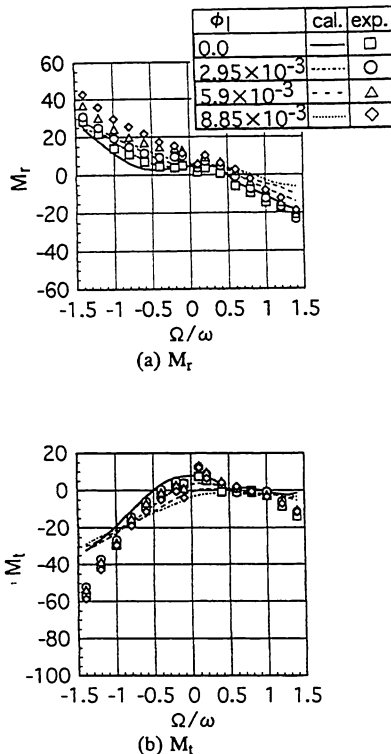


Fig. 8 Normalized moment components (effects of leakage flow rate ϕ_l , with $S = 2$ mm, uncertainty in $M_r, M_t = \pm 2$ and in $\Omega/\omega = \pm 0.002$)

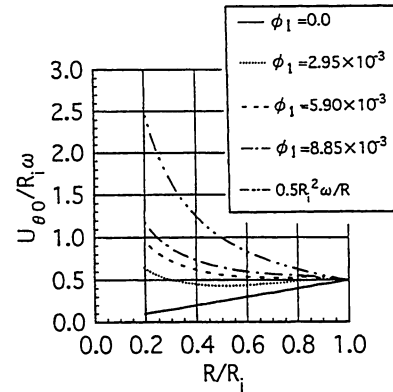


Fig. 9 Effects of leakage flow rate ϕ_l on the steady tangential velocity distribution $U_{\theta 0}(R)$

Effects of Leakage Flow Rate and the Resistance at the Leakage Flow Inlet. Figure 8 shows the effects of leakage flow rate ϕ_l . The value of $\phi_l = 2.95 \times 10^{-3}$ corresponds to 2.8 percent of design flow rate $\phi_d = 0.106$. In both calculations and experiments, M_r increases as the increase in ϕ_l , which results in the increase of the range of destabilization ($M_r > 0$ for $\Omega/\omega > 0$). Figure 9 shows the calculated steady tangential velocity distribution $U_{\theta 0}(R)$ for various leakage flow rate. As the increase in the leakage flow rate, the velocity distribution shifts from forced vortex type ($0.5R\omega$) to free vortex type ($0.5R_i^2\omega/R$) due to the angular momentum carried by the inward leakage flow. This result, as well as the result in Fig. 6, suggests that the increase in the steady tangential velocity is responsible for the destabilization.

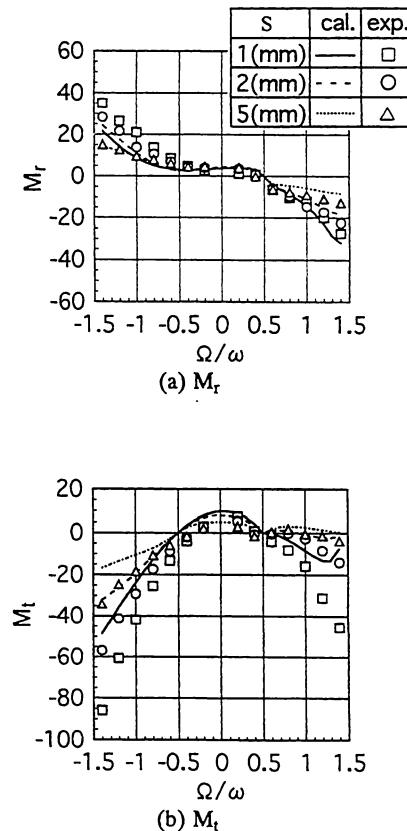


Fig. 10 Normalized moment components (effects of leakage entrance clearance S , with $\phi_l = 0$, uncertainty in $M_r, M_t = \pm 2$ and in $\Omega/\omega = \pm 0.002$)

Figure 10 shows the effects of the resistance at the leakage flow inlet. The measured pressure drop shown in Fig. 5 is used for the calculations. Both M_x and M_y generally increase as the decrease in the clearance S . This is caused by the larger value of K in Eq. (3) or the larger slope of the curves in Fig. 5 for smaller clearance S , which results in larger pressure fluctuation at the inlet of leakage flow and the larger force moment. The destabilizing fluid moment $M_x > 0$ in $0 < \Omega/\omega < 0.5$ is not so largely affected by the size of clearance.

Conclusions

The results of the present study can be summarized as follows.

- (1) The unsteady flow in the backshroud/casing clearance caused by the precessing motion is basically a 2-D inviscid flow with minor effects of unsteady wall shear stress.
- (2) The viscosity of the fluid affects the result through the steady tangential velocity distribution and the pressure loss at the leakage flow inlet.
- (3) The bulk flow model can simulate the clearance flow fairly well if we incorporate the correct behavior of the loss at the leakage flow inlet.
- (4) The inlet pressure drop was linear with the leakage flow rate rather than parabolic as usually expected.
- (5) Destabilizing fluid force moment for precessing motion is observed for small positive precessing velocity ratio.
- (6) The frequency range of destabilizing moment increases as the increase in the leakage flow rate, caused by the increase in the steady tangential velocity in the clearance.

The authors would like to acknowledge the contribution of Mr. Akira Saito in establishing the experimental procedure. This study is partly supported by the Grant-in Aid for Developmental Scientific Research (B) of the Japanese Ministry of Education, Science and Culture.

References

Adkins, D. R., and Brennen, C. E., 1988, "Analyses of Hydraulic Radial Forces on Centrifugal Pump Impellers," *ASME JOURNAL OF FLUIDS ENGINEERING*, Vol. 110, No. 1, pp. 20–28.

Bolleter, U., Wyss, A., Welte, I., and Sturchler, R., 1987, "Measurement of Hydrodynamic Interaction Matrices of Boiler Feed Pump Impellers," *ASME Journal of Vibration, Acoustics, Stress and Reliability in Design*, Vol. 109, No. 2, pp. 144–151.

Brennen, C. E., 1994, *Hydrodynamics of Pumps*, Concepts ETI, and Oxford University Press.

Childs, D. W., 1993, *Turbomachinery Rotordynamics*, Wiley, New York.

Childs, D. W., 1989, "Fluid Structure Interaction Forces at Pump-Impeller-Shroud Surfaces for Rotordynamic Calculations," *ASME Journal of Vibration, Acoustics, Stress and Reliability in Design*, Vol. 111, No. 4, pp. 216–225.

Guinzburg, A., Brennen, C. E., Acosta, A. J., and Caughey, T. K., 1994, "Experimental Results for the Rotordynamic Characteristics of Leakage Flows in Centrifugal Pump," *ASME JOURNAL OF FLUIDS ENGINEERING*, Vol. 116, No. 1, pp. 110–115.

Hirs, G. G., 1973, "A Bulk Flow Theory for Turbulence in Lubricant Film," *ASME Journal of Lubrication Technology*, Apr., pp. 137–146.

Jery, B., Acosta, A. J., Brennen, C. E., and Caughey, T. K., 1985, "Forces on Centrifugal Pump Impellers," *Proceedings of the 2nd International Pump Symposium*, Houston, Texas, pp. 21–32.

Jery, B., 1986, "Experimental Study of Unsteady Hydrodynamic Force Matrices on Whirling Centrifugal Pump Impellers," Ph.D thesis, California Institute of Technology.

Shoji, H., and Ohashi, H., 1987, "Lateral Fluid Forces on Whirling Centrifugal Impeller (1st report: Theory)," *ASME JOURNAL OF FLUIDS ENGINEERING*, Vol. 109, No. 2, pp. 94–99.

Ohashi, H., Imai, H., and Tsuchihashi, T., 1991, "Fluid Force and Moment on Centrifugal Impellers in Precession Motion," *ASME Fluid Machinery Forum*, FED-Vol. 119, pp. 57–60.

Ohashi, H., Sakurai, A., and Nishijima, J., 1988, "Influence of Impeller and Diffuser Geometries on the Lateral Fluid Forces of Whirling Centrifugal Impeller," *NASA CP 3026*, pp. 285–306.

Ohashi, H., and Shoji, H., 1987, "Lateral Fluid Forces on Whirling Centrifugal Impeller (2nd report: Experiment in Vaneless Diffuser)," *ASME JOURNAL OF FLUIDS ENGINEERING*, Vol. 109, No. 2, pp. 100–106.

Smith, D. R., Price, S. M., and Kunz, F. K., 1996, "Centrifugal Pump Vibration Caused by Supersynchronous Shaft Instability Use of Pumpout Vanes to Increase Pump Shaft Stability," *Proceedings of the 13th International Pump Users Symposium*, Houston, Texas, pp. 47–60.

Tsujimoto, Y., and Acosta, A. J., 1987, "Theoretical Study of Impeller and/or Vaneless Diffuser Attributed Rotating Stalls and Their Effects on Whirling Instability of a Centrifugal Impeller," Work Group on the Behavior of Hydraulic Machinery Under Steady Oscillatory Conditions, Lille, France.

Tsujimoto, Y., Acosta, A. J., and Brennen, C. E., 1988A, "Theoretical Study of Fluid Forces on Centrifugal Pump Impellers," *ASME Journal of Vibration, Acoustics, Stress and Reliability in Design*, Vol. 110, No. 3, pp. 263–269.

Tsujimoto, Y., Acosta, A. J. and Yoshida, Y., 1988B, "A Theoretical Study of Fluid Forces on a Centrifugal Impeller Rotating and Whirling in a Vaned Diffuser," *NASA CP 3026*, pp. 307–322.

Yamada, Y., 1962, "Resistance of Flow Through Annulus with an Inner Rotating Cylinder," *Bulletin of JSME*, Vol. 5, No. 18, pp. 301–310.

Yoshida, Y., Saito, A., Ishizaki, S., Tsujimoto, Y. and Ohashi, H., 1996, "Measurements of Flow in the Backshroud/Casing Clearance of a Precessing Centrifugal Impeller," *Proceedings of the 6th International Symposium on Transport Phenomena and Dynamics of Rotating Machinery*, Vol. 2, Honolulu, Hawaii, pp. 151–160.